Electronic Supplementary Information for

Hydrated Cation-π Interactions of π-electrons with Hydrated Li^+, Na^+, K^+ Cations

Liuhua Mu[a, b], Yizhou Yang[c], Jian Liu[d], Wei Du[a, b], Jige Chen[a, e], Guosheng Shi [f*], and Haiping Fang[c, e*]

[a.] Division of Interfacial Water and Key Laboratory of Interfacial Physics and Technology, Shanghai Institute of Applied Physics, Chinese Academy of Sciences, Shanghai 201800, China

[b.] University of Chinese Academy of Sciences, Beijing 100049, China

[c.] Department of Physics, East China University of Science and Technology, Shanghai 200237, China

[d.] School of Physical Science and Technology, ShanghaiTech University, Shanghai 201210, China

[e.] Shanghai Synchrotron Radiation Facility, Zhangjiang Laboratory, Shanghai Advanced Research Institute, Chinese Academy of Sciences, Shanghai, 201204, China

[f.] Shanghai Applied Radiation Institute and State Key Lab. Advanced Special Steel, Shanghai University, Shanghai 200444, China

***** E-mail: fanghaiping@sinap.ac.cn (H.F.); gsshi@shu.edu.cn (G.S.)

Contents:

PS1: DFT optimized geometries for hydrated cations adsorbed on a graphene sheet

Using Density Functional Theory (DFT) calculations, we carefully studied three typical alkali ions (Li^+, Na^+, K^+) based hydrated cluster adsorbed on a graphene sheet with water number ranging from 0 to 9. The graphene sheet was modeled as $C_{84}H_{24}$ (12.28 × 15.67 $Å^2$, 84 carbon atoms, and 24 hydrogen atoms) since it has been reported that this size graphene sheet was large enough to mimic the graphene surface with a tolerable error[1]. The possible geometries of the Cation-$(H_2O)_n$@Graphene, and Cation-$(H_2O)_n$ clusters at n = 0−9 for Cation = Li^+, Na^+, and K^+ are investigated. In order to find the lowest-energy structure, a large number of initial candidate geometries were determined using known hydration structures[2-7]. As the Cation-$(H_2O)_n$@Graphene, and Cation-$(H_2O)_n$ clusters become larger (n = 6-9), we performed additional structural searches using the artificial bee colony (ABC) algorithm, as implemented in the ABCluster program (version 2.0)[8, 9]. The ABC algorithm is designed to explore the potential energy surface with high efficiency by mimicking the foraging behavior of bee colonies. Its reliability and efficiency in predicting stable structures have been confirmed in previous studies[10-12]. For the Cation-$(H_2O)_n$@Graphene, and Cation-$(H_2O)_n$ clusters with n = 6−9, Grimme's tight-binding quantum chemical method GFN2-xTB (version 6.2.1)[13, 14] was adopted for local optimizations, which is computationally feasible for large-scale simulations of the ABCluster structure searches to ensure the efficient exploration of the large configurational space. In these cases, structural searching simulations for each calculation were stopped after generating 5000 structures, and these explored structures were ranked according to the calculated energy. Then the 50 lowest-energy structures were further re-optimized at the M06-2X/6-31g(d) level of theory

for both the Cation-$(H_2O)_n$@Graphene, and Cation-$(H_2O)_n$ clusters with n = 6−9. We note that the meta-GGA hybrid functional M06-2X[15, 16] can accurately describes non-covalent interactions in dispersion-dominated complexes, which has been widely used to study the systems containing aromatic ring structures[17-20].

During geometry optimizations, the graphene sheet was set free, and no symmetry restrictions were imposed at all computational methods. The total charge of each system containing alkali-cations was 1e. We performed the geometry optimizations by the Berny algorithm[21], where the convergence criterion of the maximum step size is 0.0018 au and the root mean square (RMS) force is 0.0003 au. Interaction energies were corrected for the basis set superposition error (BSSE) by using the full counterpoise method[22]. All these DFT calculations were performed using the Gaussian-09 program (Revision A.01)[23].

The relative energies (ΔE_m) between the metastable and the most stable optimized structures are defined as

$$\Delta E_m = E_m^* - E_m \tag{1}$$

where E_m^* and E_m respectively are the total energies of the metastable and the most stable optimized structures. The most stable optimized geometries of Li^+-$(H_2O)_n$@Graphene at n = 1−9 and four metastable optimized geometries of Li^+-$(H_2O)_n$@Graphene at n = 6−9 are shown in Figure S1. With the successive additions of water molecules around Li^+, there are no hydrogen bonds are formed until n = 5 for hydrated Li^+, which indicates that the water molecules tend to disperse around Li^+ without forming hydrogen bonds. Interestingly, an umbrella-like surface hydration shell is formed at n = 6 (Figure S1f), consistent with the observation in Fig. 1b that the θ values (89.61°) of Li^+ is

very close to 90˚. When $n \geq 4$, Li^+ ions tend to be fully wrapped by four water molecules, and the graphene sheet interacts with Li^+ indirectly, that is, the cation-water-π interactions. This indicates that the water molecules within the first hydration shell are tightly bound to the Li^+ cation.

The most stable optimized geometries of Na^+-$(H_2O)_n$@Graphene at n = 1−9 and four metastable optimized geometries of Na^+-$(H_2O)_n$@Graphene at n = 6−9 are shown in Figure S2. Similar to hydrated Li^+, as successively add water molecules around Na^+, there are no hydrogen bonds are formed until n = 4 for hydrated Na^+, which indicates that the water molecules tend to disperse around Na^+ without forming hydrogen bonds. In addition, an umbrella-like surface hydration shell is formed at n = 6 (Figure S2f). With further increasing n from 7 to 9, the side views in Figure s2g-i show that sodium ions located at lower than the lowest water molecules, which is consistent with the observation in Fig. 1b that the θ values of Na^+ are larger than 90˚.

Figure S3 shows that the K^+ ion tends to partial dehydrate and adsorb directly on the graphene surface as n increases from 1 to 9. With the successive additions of water molecules around the cations, there are no hydrogen bonds are formed until n = 2, 4, and 5 for hydrated K^+, hydrated Na^+, and hydrated Li^+, respectively. This indicates that the water molecules around K^+ tend to converge to form hydrogen bonds, rather than disperse around cations as the water molecules around Na^+ and Li^+ without forming hydrogen bonds. For instance, there are three hydrogen bonds are formed in the K^+-$(H_2O)_3$@Graphene, yet no hydrogen bonds are formed in Li^+ and Na^+ systems (at n = 3). Because the first shell water molecules surrounding the K^+ are comparatively more flexible and hence the hydrogen

bonds are more amenable to form.

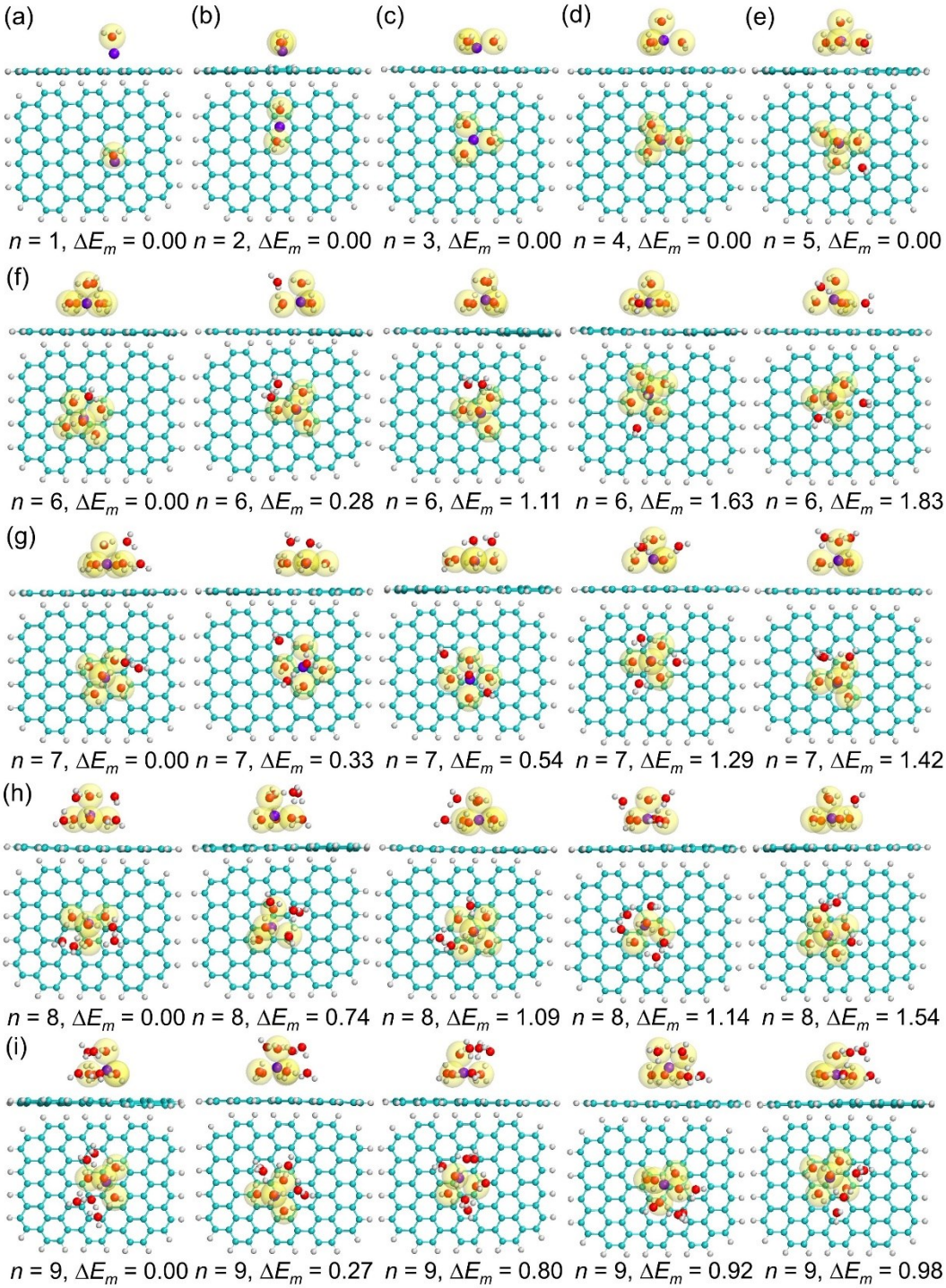

Figure S1. Most stable optimized geometries of Li^+-$(H_2O)_n$@Graphene at n = 1−9 and four metastable optimized geometries of Li^+-$(H_2O)_n$@Graphene at n = 6−9 from density functional theory calculations. Values of ΔE_m indicate the relative energies (kcal/mol). Spheres in purple, cyan, white and red represent Li^+, carbon, hydrogen, and oxygen, respectively. The transparent yellow area is the van der Waals volume of water molecules in the first hydration shell.

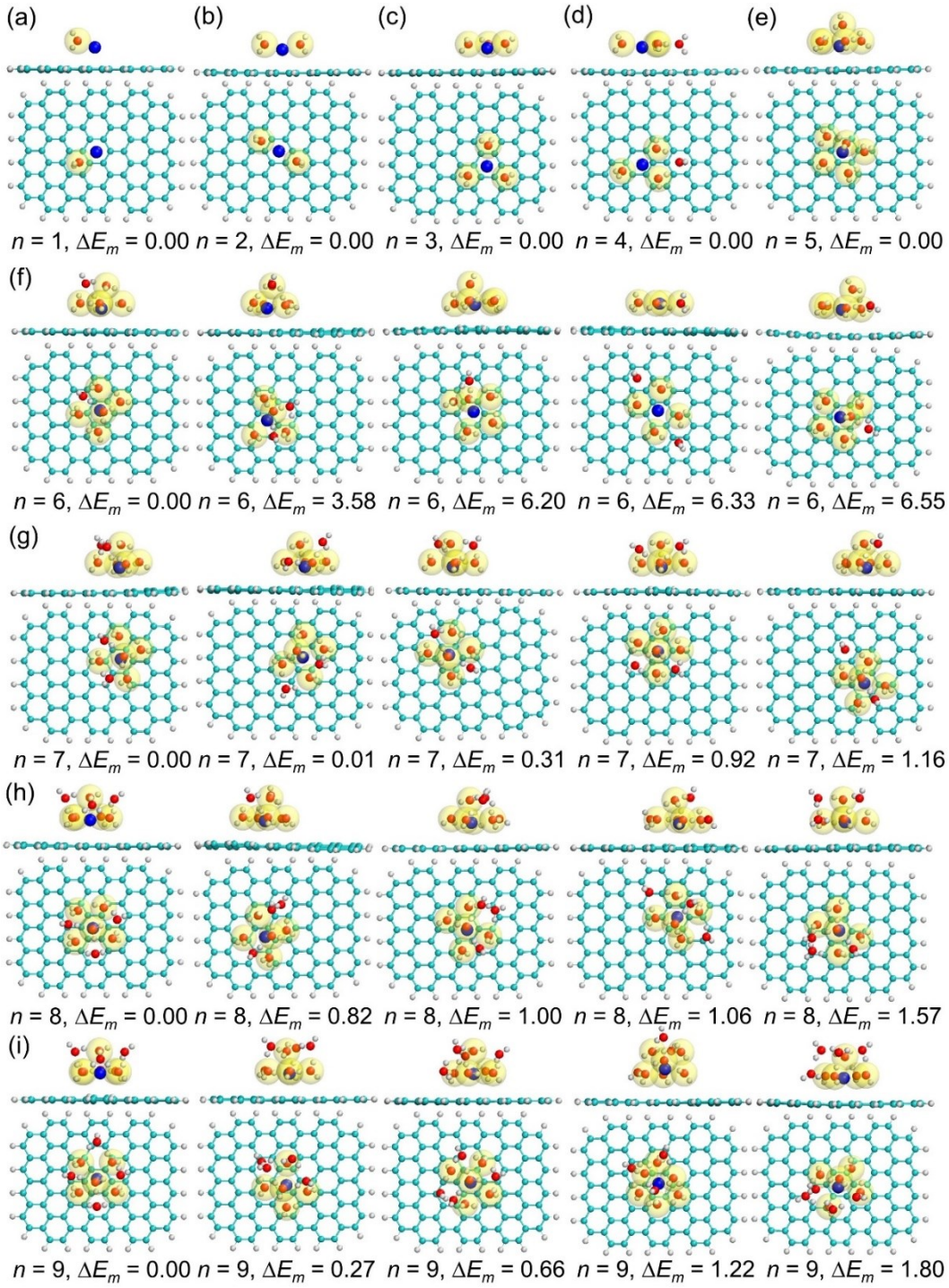

Figure S2. Most stable optimized geometries of Na^+-$(H_2O)_n$@Graphene at n = 1−9 and four metastable optimized geometries of Na^+-$(H_2O)_n$@Graphene at n = 6−9 from density functional theory calculations. Values of ΔE_m indicate the relative energies (kcal/mol). Spheres in blue, cyan, white and red represent Na^+, carbon, hydrogen, and oxygen, respectively. The transparent yellow area is the van der Waals volume of water molecules in the first hydration shell.

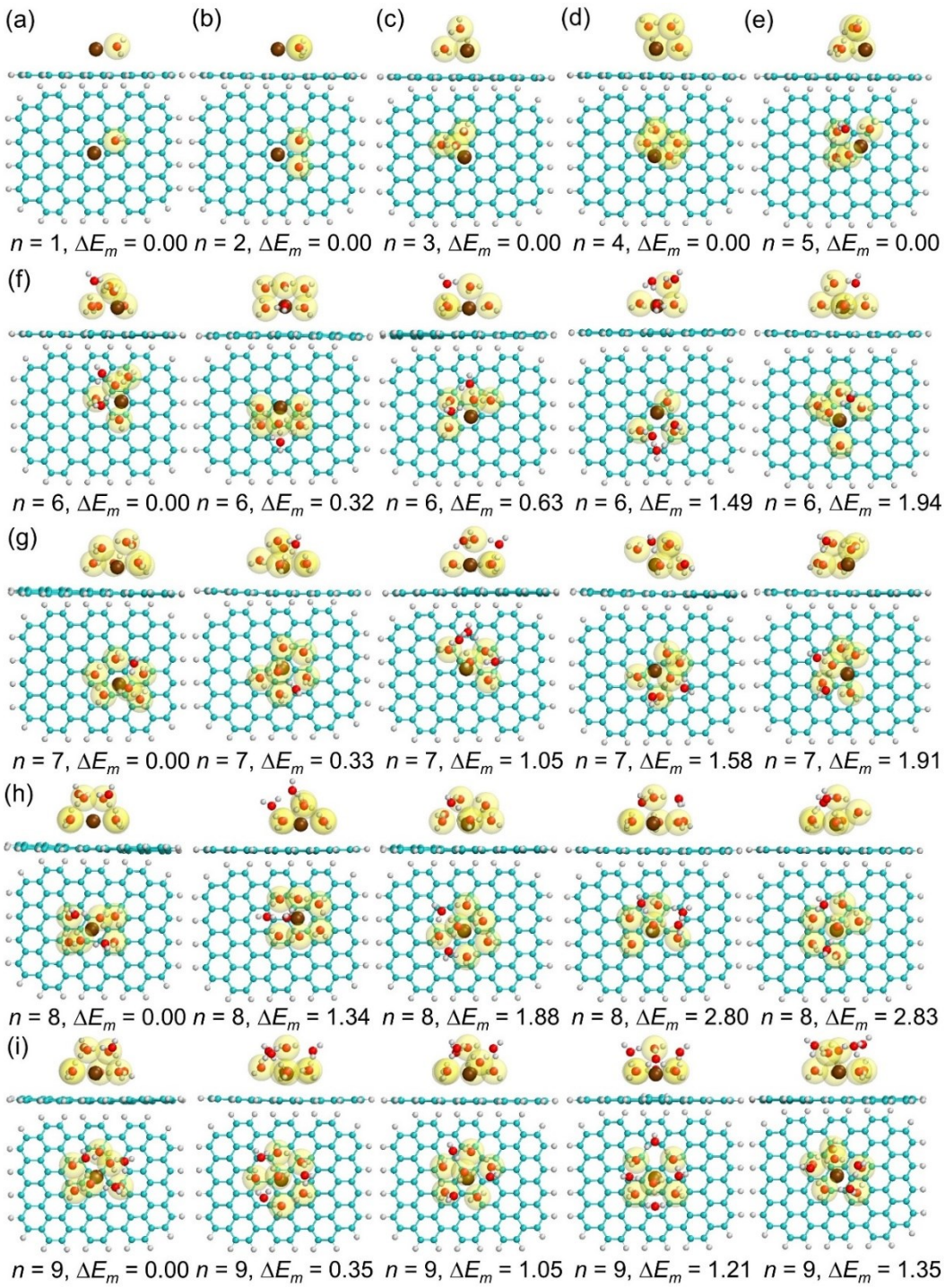

Figure S3. Most stable optimized geometries of K^+-$(H_2O)_n$@Graphene at n = 1−9 and four metastable optimized geometries of K^+-$(H_2O)_n$@Graphene at n = 6−9 from density functional theory calculations. Values of ΔE_m indicate the relative energies (kcal/mol). Spheres in brown, cyan, white and red represent K^+, carbon, hydrogen, and oxygen, respectively. The transparent yellow area is the van der Waals volume of water molecules in the first hydration shell.

PS2: DFT optimized geometries for hydrated cations

Similar to PS1, the most stable and some metastable optimized structures of Cation-$(H_2O)_n$ clusters with the labels of ΔE for Li^+, Na^+, and K^+ are respectively shown in Figure S4, S5, and S6.

Figure S4 shows the most stable optimized geometries of Li^+-$(H_2O)_n$ at n = 1−9 and four metastable optimized geometries of Li^+-$(H_2O)_n$ at n = 6−9. When $n \geq 4$, the hydrated Li^+ ions usually are fully wrapped by four water molecules, because the water molecules within the first hydration shell are tightly bound to the Li^+ cation. In contrast, the structures of K^+-$(H_2O)_n$ are quite different from that of Li^+-$(H_2O)_n$, and the K^+ ions maintain partial dehydrate as n increases from 1 to 9 (Figure S6). Note that this partial dehydration is similar to the structures of the K^+-$(H_2O)_n$@Graphene clusters, suggesting that the hydration cell of the K^+ ion is quite labile and can be clearly distorted when K^+ hydrates adsorb on the graphene surface. When compared to the Li^+ hydrates, the first hydration shell of Na^+ ion is more flexible and the water molecules surrounding Na^+ are relatively more labile. Consequently, as shown in Figure S5, the Na^+ ions maintain partial dehydrate as n increases from 1 to 7, but are fully wrapped by surrounding water molecules at n = 8, 9. These results are indicate that the hydration effects of the water molecules on the hydrated cations follow the order hydrated Li^+ > hydrated Na^+ > hydrated K^+, consistent the calculations in figure 1e that the strength of the hydration energies follows a decreasing order, hydrated Li^+ > hydrated Na^+ > hydrated K^+.

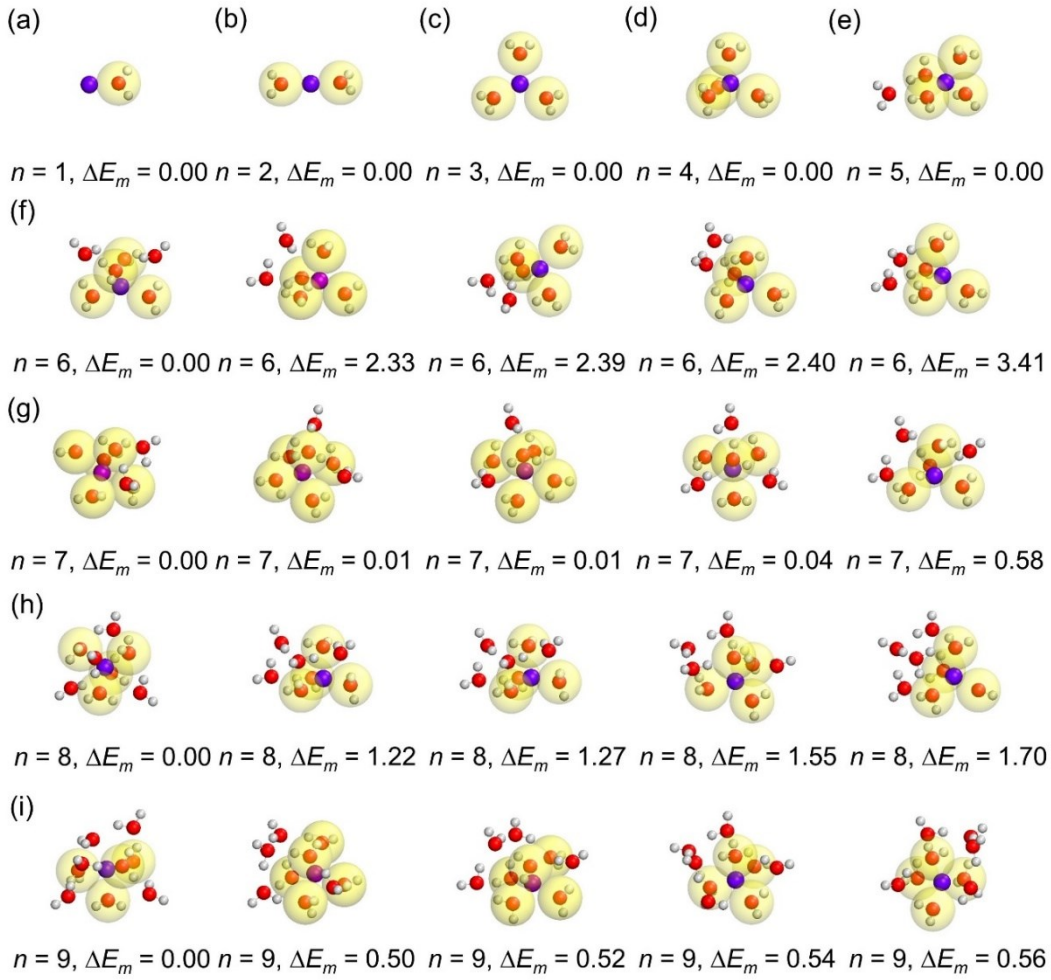

Figure S4. Most stable optimized geometries of Li^+-$(H_2O)_n$ at n = 1−9 and four metastable optimized geometries of Li^+-$(H_2O)_n$ at n = 6−9 from density functional theory calculations. Values of ΔE_m indicate the relative energies (kcal/mol). Spheres in purple, white and red represent Li^+, hydrogen, and oxygen, respectively. The transparent yellow area is the van der Waals volume of water molecules in the first hydration shell.

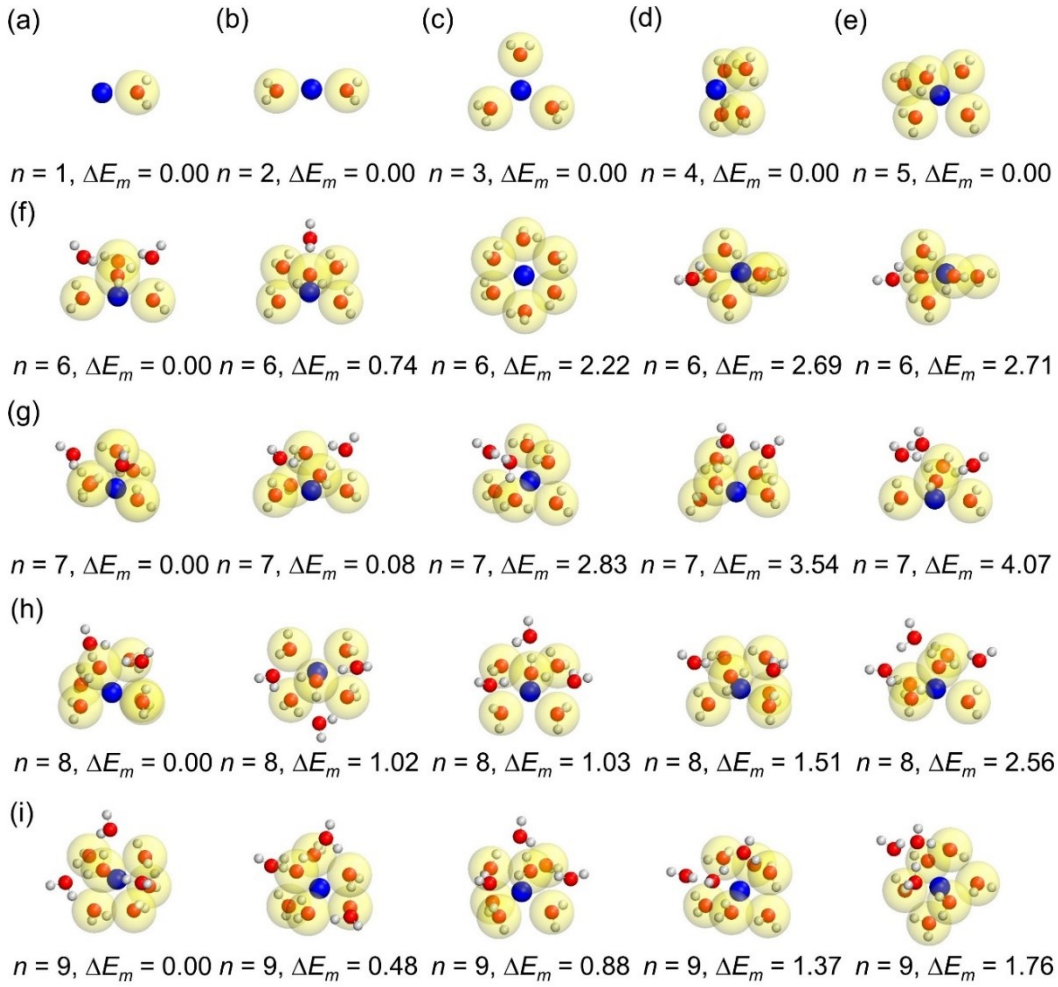

Figure S5. Most stable optimized geometries of Na^+-$(H_2O)_n$ at n = 1−9 and four metastable optimized geometries of Na^+-$(H_2O)_n$ at n = 6−9 from density functional theory calculations. Values of ΔE_m indicate the relative energies (kcal/mol). Spheres in blue, white and red represent Na^+, hydrogen, and oxygen, respectively. The transparent yellow area is the van der Waals volume of water molecules in the first hydration shell.

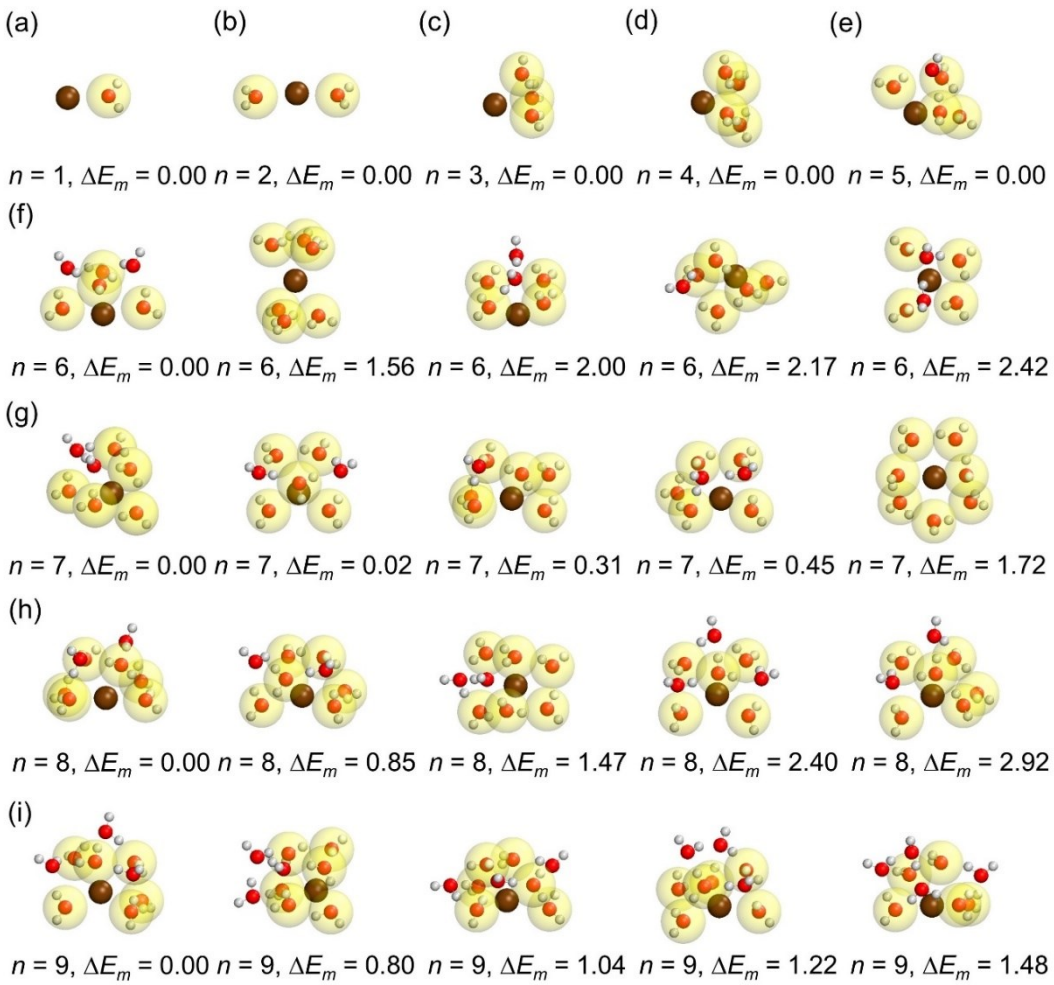

Figure S6. Most stable optimized geometries of K^+-$(H_2O)_n$ at n = 1−9 and four metastable optimized geometries of K^+-$(H_2O)_n$ at n = 6−9 from density functional theory calculations. Values of ΔE_m indicate the relative energies (kcal/mol). Spheres in brown, white and red represent K^+, hydrogen, and oxygen, respectively. The transparent yellow area is the van der Waals volume of water molecules in the first hydration shell.

PS3: Orbital analysis, electron structure analysis and Mulliken population analysis

In order to understand the underline physics of the hydrated cations on graphene, we analyzed their molecular orbitals, electron structure, and Mulliken charge distributions. We note that electron structure analysis can be obtained by calculating the total density of states (TDOS) and partial density of states (PDOS). The plots of TDOS and PDOS provide a pictorial representation of MO compositions and the contributions of fragments in the Cation-$(H_2O)_n$@Graphene, since the curves for the density of states are simulated based on the distribution of MO energy levels[24]. Figure S7a-c show three occupied molecular orbitals of three hydrated cations on graphene, demonstrating the occurrence of partial electron transfer from the delocalized π states of graphene to the unoccupied orbitals of the hydrated cations, and the plots of TDOS and PDOS reveal that the graphene sheet contributes the most to these occupied molecular orbitals. In addition, the distribution of these delocalized states is disturbed by water molecules, comparing with the molecular orbitals without water molecules (n = 0, see Figure S9). This implies that the screening effect of water molecules significantly reduces the hydrated cation-π interactions (see Figure 1d).

Furthermore, water molecules have different effects on the adsorption of different hydrated cations. Figure S7a shows that the HOMO-31 of Li^+-$(H_2O)_7$@Graphene is homogeneously distributed over the entire system, and its energy level, represented by the vertical dashed line in the below panel of PDOS plots, contains contributions from graphene and water. Consequently, there are a large number of electrons transferred from water molecules to the unoccupied orbitals of the graphene sheet, which is consistent with that the

Mulliken charge of the graphene sheet is significantly reduced from 0.43e (n = 1) to 0.08e (n = 7, see Figure S7d). This indicates that the hydrated Li^+-π interaction is strongly screened by surrounding water molecules, and the hydrated Li^+-π interactions should transit totally through the water media.

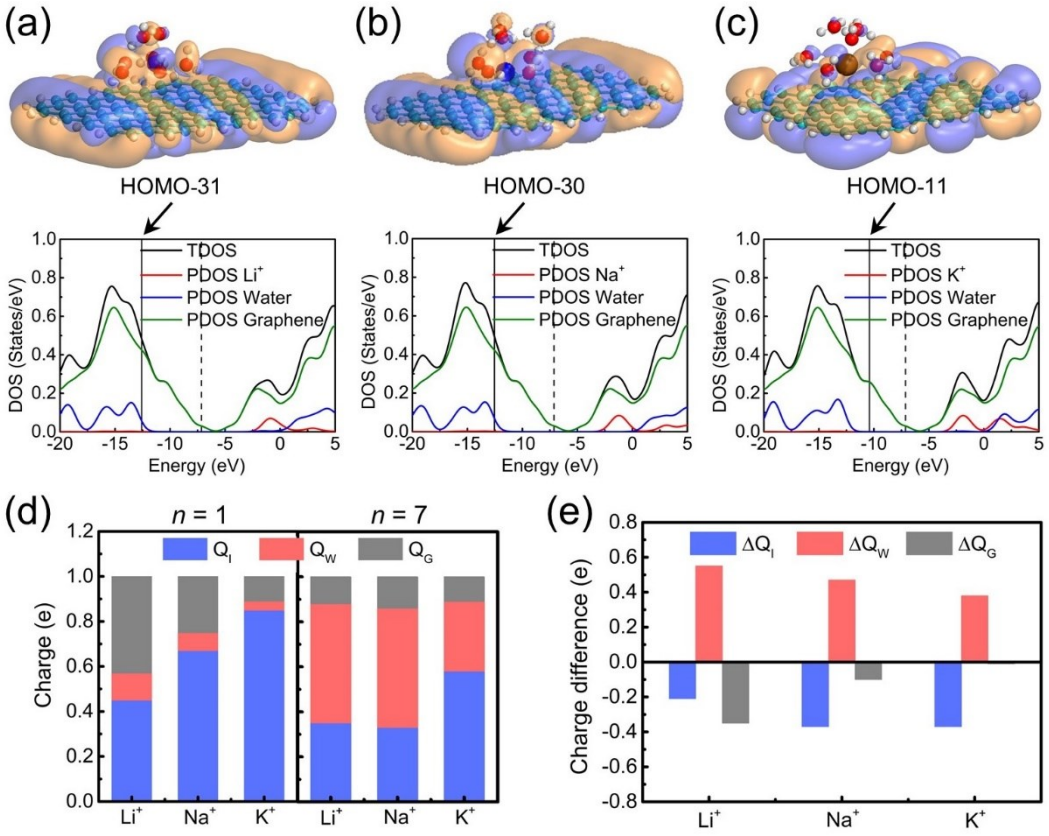

Figure S7. Orbital analysis, electron structure analysis, and Mulliken population analysis. (a), (b), and (c) are the molecular orbitals of Li^+-$(H_2O)_7$@Graphene, Na^+-$(H_2O)_7$@Graphene, and K^+-$(H_2O)_7$@Graphene at HOMO-31, HOMO-30, and HOMO-11, respectively. HOMO represents the highest occupied state of the molecular orbitals. The corresponding total density of states (TDOS) and partial density of states (PDOS) are plotted in the below panel for better comparison (the vertical dashed line indicates the position of the HOMO level). The electron density is plotted for iso-values of ±0.002 atomic units with yellow and blue denoting opposite signs. Spheres in purple, blue, brown, cyan, white, and red represent Li^+, Na^+, K^+, carbon, hydrogen, and oxygen, respectively. (d) Mulliken charges of the Cation-$(H_2O)_1$@Graphene and Cation-$(H_2O)_7$@Graphene clusters. Q_I, Q_W, and Q_G separately are the total charges of the ions, water molecules, and graphene sheets. (e)

Mulliken charge difference between $n = 7$ and $n = 1$, in which $\Delta Q_I = Q_I\ (n = 7) - Q_I\ (n = 1)$, $\Delta Q_w = Q_w\ (n = 7) - Q_w\ (n = 1)$, and $\Delta Q_G = Q_G\ (n = 7) - Q_G\ (n = 1)$.

In the case of hydrated K^+, the HOMO-11 of K^+-$(H_2O)_7$@Graphene is mainly located at the graphene sheet and the K^+ ion, and the electronic delocalization of water molecules is smaller than the case of hydrated Li^+. Moreover, the energy level of HOMO-11 in K^+-$(H_2O)_7$@Graphene only contains contributions from graphene (see the plots of PDOS in Figure S7c). In addition, Figure S7e shows that the Mulliken charge difference between $n = 7$ and $n = 1$ for the graphene sheet is quite small (ΔQ_G = -0.01e), and the absolute value of ΔQ_I (0.37e) is almost equal to that of ΔQ_W (0.38e). These imply that the water molecules can just very slightly depress partial electron transfer from the graphene sheet to the K^+ ion, even though a considerable number of electrons are transferred from water molecules to the unoccupied orbitals of the K^+ ion. For hydrated Na^+, Figure S7e shows that the amount of its Mulliken charge difference of the graphene sheet and water is intermediate between the case of hydrated Li^+ and hydrated K^+. Therefore, the screening effects of the water molecules on the hydrated cations follow the order hydrated Li^+ > hydrated Na^+ > hydrated K^+, consistent with the observations in Figure 1d that the strength of adsorption energies increase in an order of hydrated Li^+ < hydrated Na^+ < hydrated K^+ at $n = 7–9$.

We also analyzed the Mulliken charge distribution for optimized geometries of the Cation-$(H_2O)_7$@Graphene cluster (see Figure S9). From the Mulliken charge distributions and the molecular orbitals (Figure S7a-c), it is clearly shown a charge transfer between the hydrated cation and the aromatic ring structure in the graphene

sheet. This indicates that the observed strong hydrated cation-π interactions between the hydrated cations and the aromatic rings are mainly attributed to partial electron transfer from the graphene to the hydrated cations.

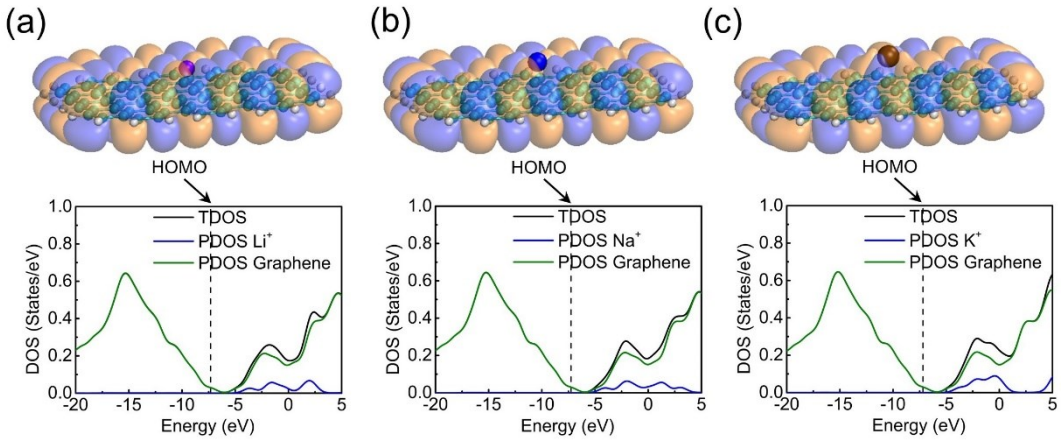

Figure S8. Orbital analysis, and electron structure analysis for optimized geometries of Cation@Graphene with Cation = Li^+, Na^+, K^+. (a), (b), and (c) are highest occupied state of the molecular orbitals (HOMO) of Li^+@Graphene, Na^+@Graphene, and K^+@Graphene, respectively. The corresponding total density of states (TDOS) and partial density of states (PDOS) are plotted in the below panel for better comparison (the vertical dashed line indicates the position of the HOMO level). The electron density is plotted for iso-values of ±0.002 atomic units with yellow and blue denoting opposite signs. Spheres in purple, blue, brown, cyan, and white represent Li^+, Na^+, K^+, carbon, and hydrogen, respectively.

Figure S8a-c show the molecular orbitals and density of states of the graphene with Li^+, Na^+, and K^+, respectively. We note that electron structure analysis can be obtained by calculating the total density of states (TDOS) and partial density of states (PDOS). The plots of TDOS and PDOS provide a pictorial representation of MO compositions and the contributions of fragments in the Cation-$(H_2O)_n$@Graphene, since the curves for the density of states are simulated based on the distribution of MO energy levels[24]. There is a clear coupling and hybridization between the delocalized π states of the aromatic ring structure in the graphene surface and the acceptor orbitals of Li^+, Na^+, and K^+, as shown in their highest occupied state of the molecular orbitals (HOMO). Moreover, the energy level of

HOMO in Cation@Graphene only contains contributions from graphene (Figure S8). We also analyzed the Mulliken charge distributions of the Cation-$(H_2O)_7$@Graphene clusters, as shown in Figure S8. The residuary Mulliken charges of Li^+, Na^+, and K^+ are 0.24e, 0.30e, and 0.48e at n = 7, respectively, as shown in Table S1. As shown in Figure S8, it is clearly shown a charge transfer between the hydrated cations and the aromatic ring structure in the graphene sheet.

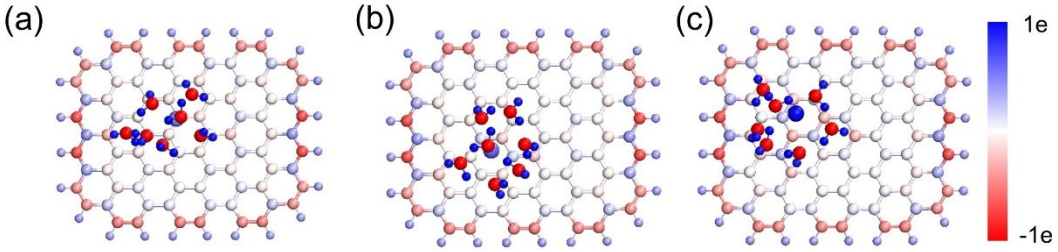

Figure S9. Mulliken population analysis for optimized geometries of Cation-(H2O)$_7$@Graphene with Cation = Li^+, Na^+, K^+. (a), (b), and (c) are Mulliken charge distributions of Li^+-$(H_2O)_7$@Graphene, Na^+-$(H_2O)_7$@Graphene, and K^+-$(H_2O)_7$@Graphene, respectively.

Table S1. Residuary Mulliken charges of Cation-$(H_2O)_n$@Graphene (n = 0−9) clusters.

n	Li^+			Na^+			K^+		
	Ion	*Water*	*G*	*Ion*	*Water*	*G*	*Ion*	*Water*	*G*
0	0.53	-	0.47	0.71	-	0.29	0.89	-	0.11
1	0.45	0.12	0.43	0.67	0.08	0.25	0.85	0.04	0.11
2	0.50	0.22	0.28	0.65	0.15	0.20	0.80	0.09	0.10
3	0.40	0.41	0.20	0.58	0.24	0.17	0.76	0.15	0.09
4	0.38	0.51	0.11	0.58	0.28	0.14	0.69	0.21	0.09
5	0.36	0.53	0.11	0.35	0.49	0.16	0.64	0.26	0.10
6	0.25	0.64	0.11	0.29	0.55	0.16	0.61	0.29	0.10
7	0.24	0.67	0.08	0.30	0.55	0.15	0.48	0.42	0.10
8	0.22	0.69	0.09	0.25	0.61	0.15	0.46	0.46	0.09
9	0.20	0.71	0.09	0.27	0.60	0.14	0.36	0.55	0.09

PS4: DFT optimized geometries for hydrated cations adsorbed on a graphene sheet with Stone-Wales (SW) defect

To explore the effect of the defect in graphene on the hydrated cation-π interactions, we performed DFT calculations for the adsorption of the hydrated cations on a graphene-SW sheet (denoted as Cation-$(H_2O)_7$@Graphene-SW). In order to find the lowest-energy structure of Cation-$(H_2O)_7$@Graphene-SW, we performed additional structural searches using the artificial bee colony (ABC) algorithm, as implemented in the ABCluster program (version 2.0)[8, 9]. Grimme's tight-binding quantum chemical method GFN2-xTB (version 6.2.1)[13, 14] was adopted for local optimizations, which is computationally feasible for large-scale simulations of the ABCluster structure searches to ensure the efficient exploration of the large configurational space. In these computations, structural searching simulations for each calculation were stopped after generating 5000 structures, and these explored structures were ranked according to the calculated energy. Then the 50 lowest-energy structures were further re-optimized at the M06-2X/6-31g(d) level of theory for Cation-$(H_2O)_7$@Graphene-SW. The most stable optimized structures and four metastable optimized structures of the Cation-$(H_2O)_7$@Graphene-SW clusters with Cation = Li^+, Na^+, and K^+ are displayed in Figure S10.

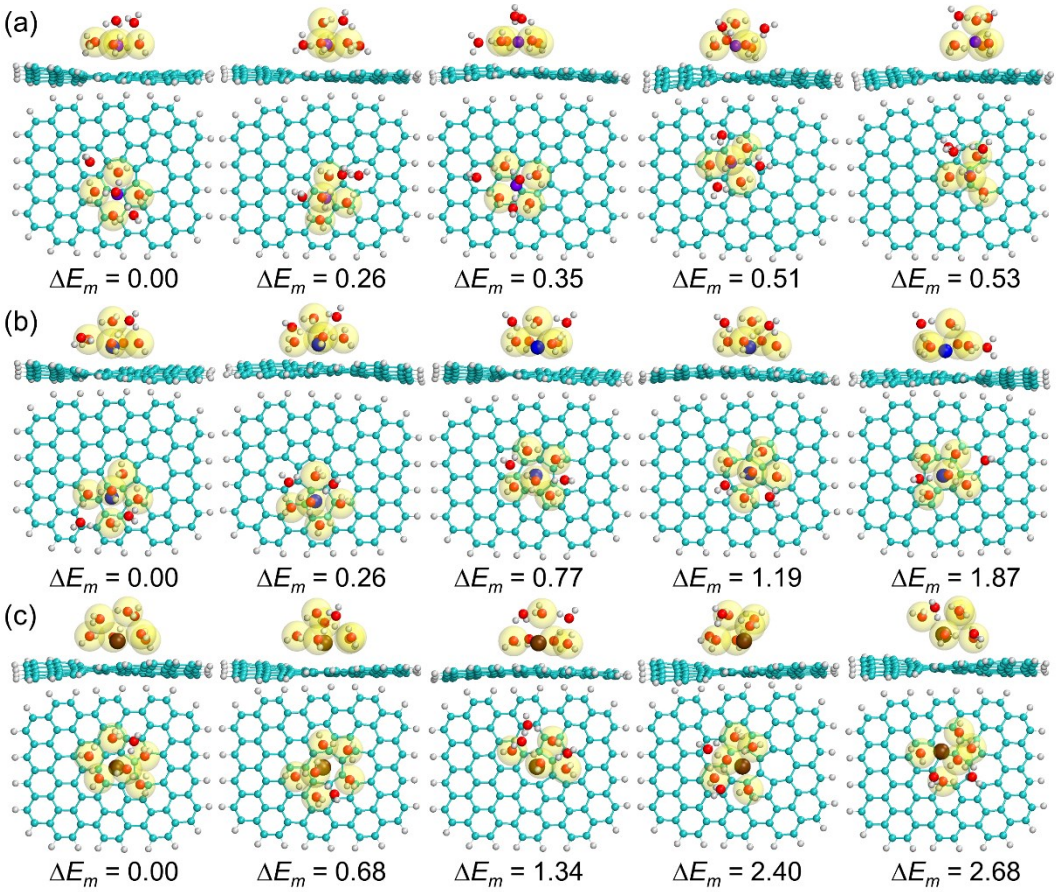

Figure S10. Most stable optimized geometries and four metastable optimized geometries of Cation-$(H_2O)_7$@Graphene-SW with Cation = Li^+, Na^+, and K^+, from density functional theory calculations. Values of ΔE_m indicate the relative energies (kcal/mol), as defined in equation 1 in PS1. Spheres in purple, blue, brown, cyan, white and red represent Li^+, Na^+, K^+, carbon, hydrogen, and oxygen, respectively. The transparent yellow area is the van der Waals volume of water molecules in the first hydration shell.

PS5: Ab initio molecular dynamics (AIMD) simulations

We firstly simulate the liquid water/graphene interface by inserting 101 water molecules between the two graphene planes in a periodic box with the dimensions 12.84 × 12.40 × 23.90 $Å^3$, which based on the previous work by Cicero et al[25, 26] and on our own tests, as shown in Figure S11a. To obtain a converged value of the energy of the system with a reasonable computational cost, we ran some tests to determine the optimal value of the energy cutoff. Figure S11b displays the energy of the system for different energy cutoffs. The chosen value, 475 Ry, produces a converged value of the energy with a reasonable computational cost. *Ab initio* molecular dynamics (AIMD) simulations for the liquid water/graphene interface have been performed at room temperature (298 K) with a time step of 0.5 fs. After equilibrating the system by 3.0 ps, the trajectories lasting 5.0 ps long were collected for calculating the density profile of water. This system presents a wide enough water bulk region with a water density of ~1.0 g/cm^3 at the central part of the graphene sheets (see Figure S11c), which ensures a proper investigation of the cations−graphene interaction in aqueous solution.

We then performed AIMD simulations for the hydrated cations/graphene interface to evaluate the temperature effect on the hydrated cation-π interaction. In order to obtain appropriate water-cation and water-surface contacts, we firstly prepared the simulation system containing fixed cations at a distance of 3.0 Å from the graphene, as displayed in Figure S11d. After equilibrating the system for 6.0 ps, the cations were set free and the final structure was then used as input for further AIMD simulations.

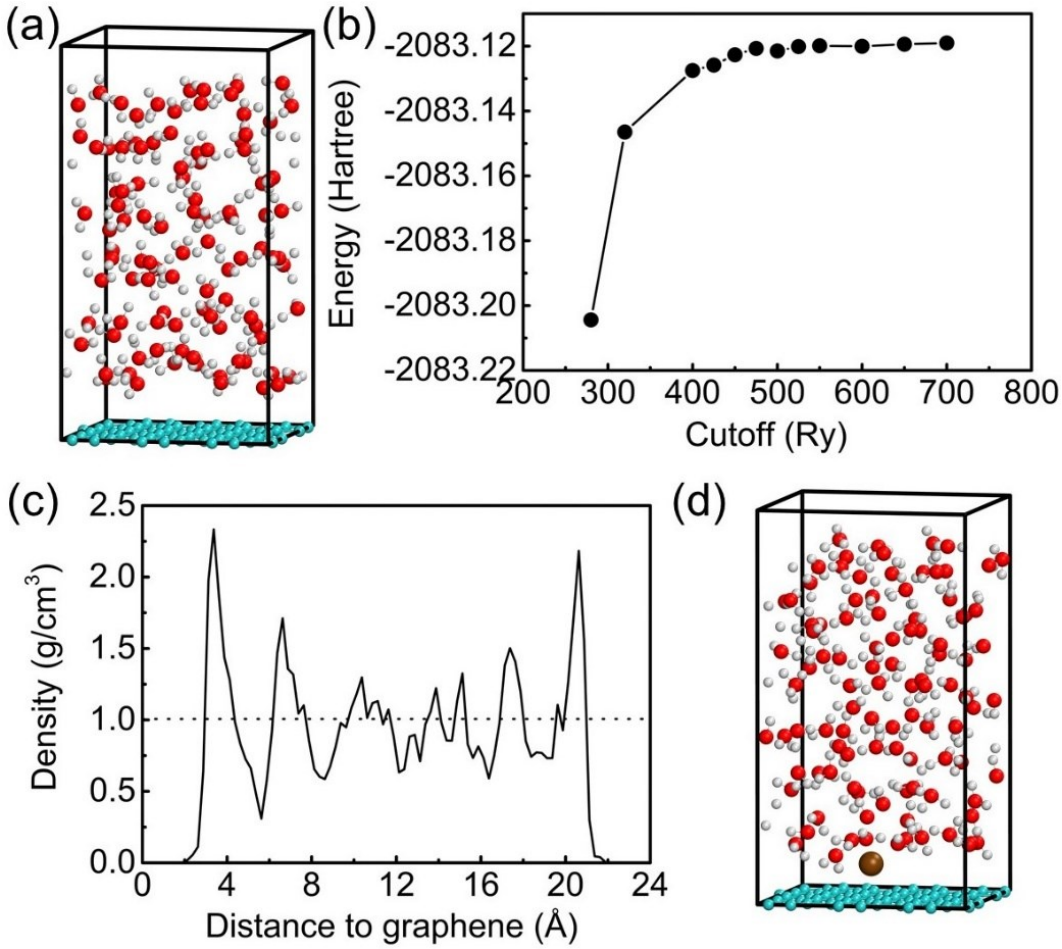

Fig. S11 *Ab initio* molecular dynamics (AIMD) simulations of the liquid water/graphene interface. (a) Snapshot of the simulation box for the liquid water/graphene interface. (b) Convergence of the energy of the system for different energy cutoffs. (c) Density profile of water obtained from the AIMD simulations. A large bulk region is present in the central part between the two graphene planes. (d) Snapshot of the simulation box for the hydrated cations/graphene interface. Spheres in brown, cyan, white and red represent cations, carbon, hydrogen, and oxygen, respectively.

ESI References

1 G.-S. Shi, Z.-G. Wang, J.-J. Zhao, J. Hu and H.-P. Fang, *Chinese Physics B*, 2011, **20**, 068101.

2 H. M. Lee, P. Tarakeshwar, J. Park, M. R. Kołaski, Y. J. Yoon, H.-B. Yi, W. Y. Kim and K. S. Kim, *The Journal of Physical Chemistry A*, 2004, **108**, 2949-2958.

3 B. S. González, J. Hernández-Rojas and D. J. Wales, *Chem. Phys. Lett.*, 2005, **412**, 23-28.

4 J. S. Rao, T. C. Dinadayalane, J. Leszczynski and G. N. Sastry, *J. Phys. Chem. A*, 2008, **112**, 12944-12953.

5 M. Mitani and Y. Yoshioka, *Journal of Molecular Structure: THEOCHEM*, 2009, **915**, 160-169.

6 O. Ouni, N. Derbel, N. Jaïdane and M. F. Ruiz-López, *Computational and Theoretical Chemistry*, 2012, **990**, 209-213.

7 E. A. Gomaa, M. A. Tahoon and A. Negm, *J. Mol. Liq.*, 2017, **241**, 595-602.

8 J. Zhang and M. Dolg, *Phys. Chem. Chem. Phys.*, 2015, **17**, 24173-24181.

9 J. Zhang and M. Dolg, *Phys. Chem. Chem. Phys.*, 2016, **18**, 3003-3010.

10 J. Li, S. Zhou, J. Zhang, M. Schlangen, D. Usharani, S. Shaik and H. Schwarz, *J. Am. Chem. Soc.*, 2016, **138**, 11368-11377.

11 G. L. Hou, J. Zhang, M. Valiev and X. B. Wang, *Phys. Chem. Chem. Phys.*, 2017, **19**, 10676-10684.

12 S. A. Akhade, A. Winkelman, V. Lebarbier Dagle, L. Kovarik, S. F. Yuk, M.-S. Lee, J. Zhang, A. B. Padmaperuma, R. A. Dagle, V.-A. Glezakou, Y. Wang and R. Rousseau, *J. Catal.*, 2020, **386**, 30-38.

13 S. Grimme, C. Bannwarth and P. Shushkov, *Journal of Chemical Theory and Computation*, 2017, **13**, 1989-2009.

14 C. Bannwarth, S. Ehlert and S. Grimme, *J Chem Theory Comput*, 2019, **15**, 1652-1671.

15 Y. Zhao and D. G. Truhlar, *Acc. Chem. Res.*, 2008, **41**, 157-167.

16 Y. Zhao and D. G. Truhlar, *Theor. Chem. Acc.*, 2007, **120**, 215-241.

17 X. P. Fu, X. S. Xue, X. Y. Zhang, Y. L. Xiao, S. Zhang, Y. L. Guo, X. Leng, K. N. Houk and X. Zhang, *Nat Chem*, 2019, **11**, 948-956.

18 M. Schwarze, C. Gaul, R. Scholz, F. Bussolotti, A. Hofacker, K. S. Schellhammer, B. Nell, B. D. Naab, Z. Bao, D. Spoltore, K. Vandewal, J. Widmer, S. Kera, N. Ueno, F. Ortmann and K. Leo, *Nat Mater*, 2019, **18**, 242-248.

19 X. Qi, Y. Li, R. Bai and Y. Lan, *Acc. Chem. Res.*, 2017, **50**, 2799-2808.

20 Y. Yang, L. Mu, L. Chen, G. Shi and H. Fang, *Phys. Chem. Chem. Phys.*, 2019, **21**, 7623-7629.

21 C. Y. Peng, P. Y. Ayala, H. B. Schlegel and M. J. Frisch, *J. Comput. Chem.*, 1996, **17**, 49-56.

22 S. F. Boys and F. Bernardi, *Mol. Phys.*, 2006, **19**, 553-566.

23 M. J. T. Frisch, G. W.; Schlegel, H. B. et al.

24 J. Feng, H. Dong, B. Pang, F. Shao, C. Zhang, L. Yu and L. Dong, *Phys. Chem. Chem. Phys.*, 2018, **20**, 15244-15252.

25 C. Calero, J. Marti, E. Guardia and M. Masia, *J Chem Theory Comput*, 2013, **9**, 5070-5075.

26 G. Cicero, J. C. Grossman, E. Schwegler, F. Gygi and G. Galli, *J. Am. Chem. Soc.*, 2008, **130**, 1871-1878.